Journal of Physics B: Atomic, Molecular and Optical Physics

Attosecond pulse generation at ELI-ALPS 100 kHz repetition rate beamline

OPEN ACCESS
IOP Publishing
Journal of Physics B: Atomic, Molecular and Optical Physics
J. Phys. B: At. Mol. Opt. Phys. **53** (2020) 154004 (11pp)
https://doi.org/10.1088/1361-6455/ab92bf

Attosecond pulse generation at ELI-ALPS 100 kHz repetition rate beamline

Peng Ye[1,10], Tamás Csizmadia[1,10], Lénárd Gulyás Oldal[1], Harshitha Nandiga Gopalakrishna[1,11], Miklós Füle[1], Zoltán Filus[1], Balázs Nagyillés[1], Zsolt Divéki[1], Tímea Grósz[1], Mathieu Dumergue[1], Péter Jójárt[1], Imre Seres[1], Zsolt Bengery[1], Viktor Zuba[1,12], Zoltán Várallyay[1], Balázs Major[1], Fabio Frassetto[2], Michele Devetta[3], Giacinto Davide Lucarelli[3,4], Matteo Lucchini[3,4], Bruno Moio[3,4], Salvatore Stagira[3,4], Caterina Vozzi[3], Luca Poletto[2], Mauro Nisoli[3,4], Dimitris Charalambidis[1,5], Subhendu Kahaly[1,6], Amelle Zaïr[1,7,9] and Katalin Varjú[1,8,9]

[1] ELI-ALPS, ELI-HU Non-Profit Ltd., Wolfgang Sandner utca 3., Szeged, H-6728, Hungary
[2] Institute for Photonics and Nanotechnologies, IFN-CNR, via Trasea 7, 35131 Padova, Italy
[3] Institute for Photonics and Nanotechnologies, IFN-CNR, 20133 Milano, Italy
[4] Department of Physics, Politecnico di Milano, 20133 Milano, Italy
[5] Foundation for Research and Technology Hellas (FORTH-IESL) PO Box 1385, 711 10 Heraklion, Greece
[6] Institute of Physics, University of Szeged, Dóm tér 9, Szeged 6720, Hungary
[7] King's College London, Attosecond Physics Group, Department of Physics, WC2R 2LS, London, United Kingdom
[8] Department of Optics and Quantum Electronics, University of Szeged, Dóm tér 9, Szeged 6720, Hungary

E-mail: amelle.zair@kcl.ac.uk and Varju.Katalin@eli-alps.hu

Received 24 March 2020, revised 4 May 2020
Accepted for publication 13 May 2020
Published 26 June 2020

Abstract

We generate attosecond pulse train (APT) in argon driven by the high repetition rate (HR) laser of the extreme light infrastructure-attosecond light pulse source (ELI-ALPS), providing 100 kHz, 80 W, 1030 nm, 40 fs pulses from a fiber chirped-pulse amplification (fiber-CPA) laser system. Under the current operating conditions of the high harmonic generation beamline (HR-GHHG), we observed the average pulse duration to be 395 as measured using the technique of reconstruction of attosecond beating by interference of two-photon transitions. The beamline uses an annular-shape laser beam so that the main part of the driving laser co-propagating with the APT can be eliminated by reflection on a holey mirror. An additional 100 nm aluminum foil is used to filter out the remaining laser and the low order harmonics, allowing 2 pJ APT with a bandwidth from 25 eV to 50 eV to be transported to the target position where the APT interacts with matter. The implementation of the HR-GHHG beamline in ELI-ALPS delivering attosecond pulse trains at 100 kHz paves the way for time-resolved

[9] Authors to whom any correspondence should be addressed.
[10] These authors contributed equally to this work.
[11] Present address: Institute of Optics and Quantum Electronics, Friedrich Schiller University, Max-Wien-Platz 1, 07743 Jena, Germany.
[12] Present address: Zepler Institute for Photonics and Nanoelectronics, University of Southampton, Southampton, United Kingdom.

experiments in the infrastructure, especially those that involve rare events and coincidence analysis, both of which need high statistics.

Keywords: high-order harmonics generation, high repetition rate, attosecond

(Some figures may appear in colour only in the online journal)

1. Introduction

The emergence of attosecond pulses [1, 2] enabled scientists entering a new era, in which one can observe, trace, and control the fastest events in matter with unprecedented—attosecond (as)—temporal resolution [3–11]. Over the past twenty years, attosecond pulses were used as a fast camera shutter to resolve and investigate ultrafast dynamical events [12–14], such as time delay of photoemission [15, 16], electron dynamics in molecules [17, 18], electron–electron correlation in strong-field [19, 20], dynamics of nanoparticles excited by few cycle laser [21–24], petahertz electronics in gas [25] and solid [26] with unprecedented temporal accuracy down to 10 as [27, 28], chemical reactions [29, 30], coincidence information of ultrafast mass spectroscopy [31], and probing strong field quantum optics in gaseous [32] and condensed matter [33]. However, until now the repetition rate of most of the attosecond sources was limited to few kHz, which hindered many applications. Using high repetition rate table-top systems, one can capture photo-induced rare events in matter and supply sophisticated time resolved measurements with all together high temporal accuracy and high signal to noise ratio. In addition, to avoid space-charge effects in attosecond pulse induced interactions, while collecting photoelectrons and ions, the XUV flux has to be limited; thus the signal-to-noise ratio can only be improved by increasing the repetition rate of the attosecond pulses. High repetition rate coherent light sources are also particularly important in coincidence measurements [34–37], where the momentum conservation law is used to reconstruct the initial energy distribution of electrons and ions. Therefore, one has to ensure that these particles are released from the same ionization event by limiting the flux to less than one ionization event per laser shot [38, 39].

High harmonic generation (HHG) is one of the main table-top methods to generate attosecond pulses [52–54]. The process can be understood as three steps on the microscopic level [55, 56]. Firstly, a strong laser field suppresses temporally the Coulomb potential of an atom or a molecule, then an electronic wave packet can tunnel into the continuum, and then it is accelerated in the driving laser field. Whilst the driving laser field reverses, the electronic wave packet is pulled back to the atomic or molecular core to interfere with the residual bound electronic wave packet in the ground state of the system. Finally, the interference results in the emission of a burst of coherent photons, whose photon energies are tens to thousands of eV [57–59]. By confining the emission time of the photon burst one can produce pulses with attosecond duration. Since such confined emission can happen in every half cycle of the strong laser field, the generation process can yield either an isolated attosecond pulse (IAP) [2, 60] or an attosecond pulse train (APT) [1, 61].

APT generation is generally easier and more efficient than the generation of IAP. The later needs CEP stabilized few-cycle laser pulses which are not always available in many laboratories, and the gating techniques [62, 63] which reduce the energy of the driving laser beam. IAP and APT can be used in different pump-probe experiments depending on specific aims. In an infrared (IR) pulse/IAP experiment the IR pulse triggers a process in a system and a delayed IAP probes the change of the system. By changing the delay the evolution of the process after the trigger event can be investigated. In comparison, since the attosecond pulses in an APT are synchronized with each half-cycle of the driving laser, in an IR/APT experiment one can investigate the cycle of the charge excitation in a system, for instance [61]. Besides, unlike an IAP, which has a continuous spectrum, an APT has a comb-like spectrum that can be used to identify different photoionization channels [64, 65]. The last advantage is that the intensity of IR in an APT experiment (RABBITT) is lower than that in an IAP experiment (streaking) [66]. The lower intensity perturbs the system less and can reduce the background of low energy electrons generated by above threshold ionization. In the studies of photoemission delays in solids, those features together with the discrete APT spectrum greatly help the experimental realization [67–69]. In addition APT allowes for direct extraction of IAPs through a combination of wave front rotation and spatial filtering methodologies using light house techniques [70]. Because of the above-mentioned practical advantages, firstly APT was generated and characterized with our beamline that is presented in this manuscript. Nevertheless, it has to be noted that the beamline will be upgraded with the possibility to generate single attosecond pulses using the polarization gating technique in the coming future, ensuring the availability of both attosecond pulse forms depending on the requirements of the given user experiment.

Until now, several high harmonic sources with high repetition rate were already built in academic laboratories. High repetition rate HHG was achieved employing intra cavity geometry carrying laser energy per pulse lower than $\sim\mu$J [41, 46, 71]. With thin-disk oscillators [44], titanium-sapphire regenerative amplifiers [72, 73] and optical parametric chirped-pulse amplification (OPCPA) [74, 75], laser pulse energy was reported as $\sim\mu$J and could produce HHG in tight focusing geometry.

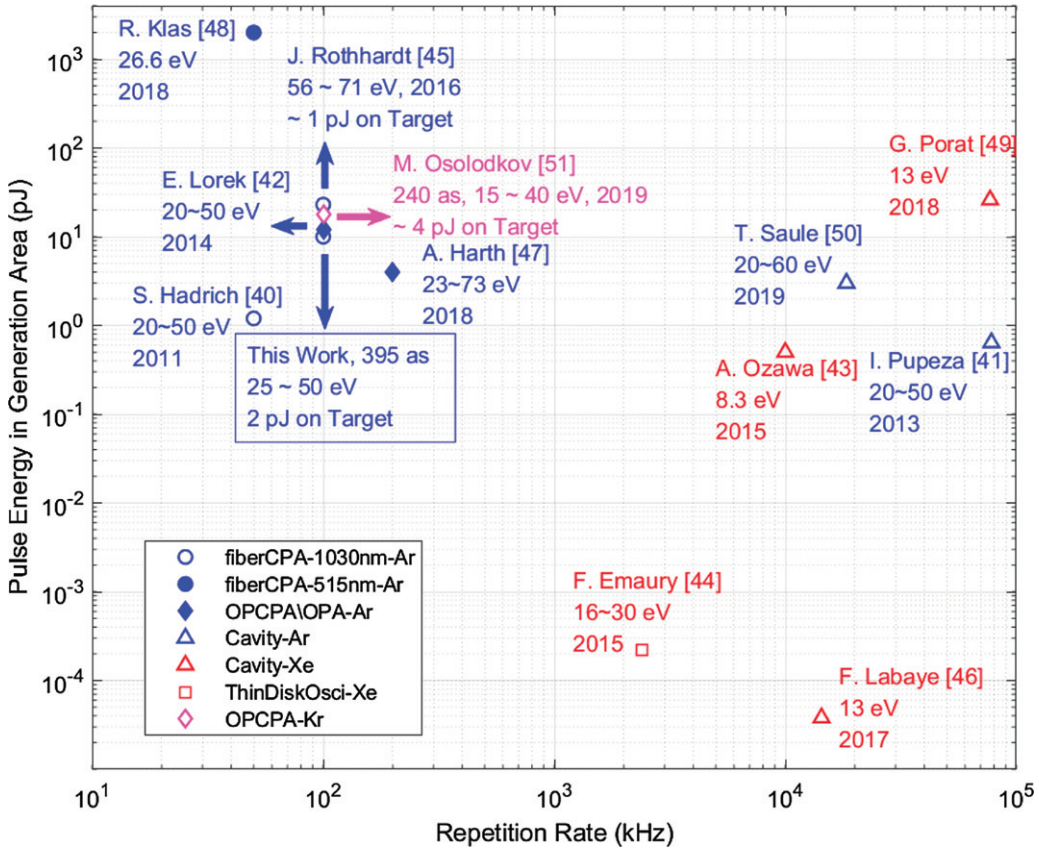

Figure 1. The pulse energy in the generation area of high repetition rate XUV sources demonstrated above 50 kHz [40–51]. The pulse energy delivered to the target position, where the high-order harmonics interact with the matter, is shown in the text. The media for HHG are argon (blue), xenon (red), and krypton (magenta). Circle: fiber-CPA. Triangle: cavity. Square: thin-disk oscillator. Diamond: OPCPA.

State-of-the-art HHG sources operate typically at repetition rates up to 1 kHz in the photon energy range from several tens of eV to the water window [8, 59, 60, 76, 77] with pulse duration as short as 50 as [7, 8]. To build an attosecond beamline with a high repetition rate there are two main challenges. Firstly, driving pulse energy in the ∼mJ level is needed. Most attosecond experiments operate in cross-correlation pump-probe schemes with a delayed replica of the generating laser pulse: (i) the attosecond pulses are generated by the main beam (generation beam) with peak intensity of few 10^{14} W cm^{-2}; (ii) the other synchronized and delayed beam (probe beam), contains usually peak intensity higher than $\sim 10^{11}$ W cm^{-2}. Recent progress in laser technology permits the production of laser pulses at high repetition rate, with energy in the mJ range, able to drive tabletop HHG, based on fiber-CPA (chirped pulse amplification) technique [40, 74, 78–83], and OPCPA [82, 84, 85] with sub-mJ pulse energy, pumped by fiber-CPA and/or thin-disk laser. These high-average power lasers allowed the generation of high repetition rate attosecond pulses in gas. The pulse energy of the high-harmonics at the generation point is reported in figure 1. In specific experiments different focusing arrangements and filters are used for the selection of the specific spectral range and elimination of the residual driving laser while delivering the high-harmonics to the target. Thus, the pulse energy on the target can vary between 95% and 1% of the pulse energy in the generation area, therefore in the view of application one should compare the usable pulse energy—pulse energy on target. However, because few articles gave this data, we compare the pulse energy at the generation point instead. For the three works which provided the energies on target, we marked them in the corresponding legend of the data entries. The method of intra-cavity generation gives a higher repetition rate in the MHz regime, but with lower pulse energy of the high-harmonics. Using fiber-CPA or OPCPA laser systems, high-harmonics with energies of several pJ can be achieved at a moderate repetition rate of ∼100 kHz. Since the energy conversion efficiency of HHG in different gases is very different, in order to make a reasonable comparison we only reported the works utilizing fiber-CPA using argon gas. We generated lower pulse energy (∼9 pJ) than what is reported in Rothhardt's work (∼23 pJ) [45], however, we deliverred higher pulse energy to the target area. Only the work of Osolodkov *et al* [51] and this work from the ones listed in figure 1 reported the durations of the high-order harmonic pulses, thus confirming the generation of attosecond pulses.

Secondly, for time-resolved studies in the pump-probe scheme, the generated attosecond pulses need to be separated from the driving laser. The well-established method of using metallic filters becomes problematic when high-power high-repetition-rate lasers are used, as filters burn due to the high

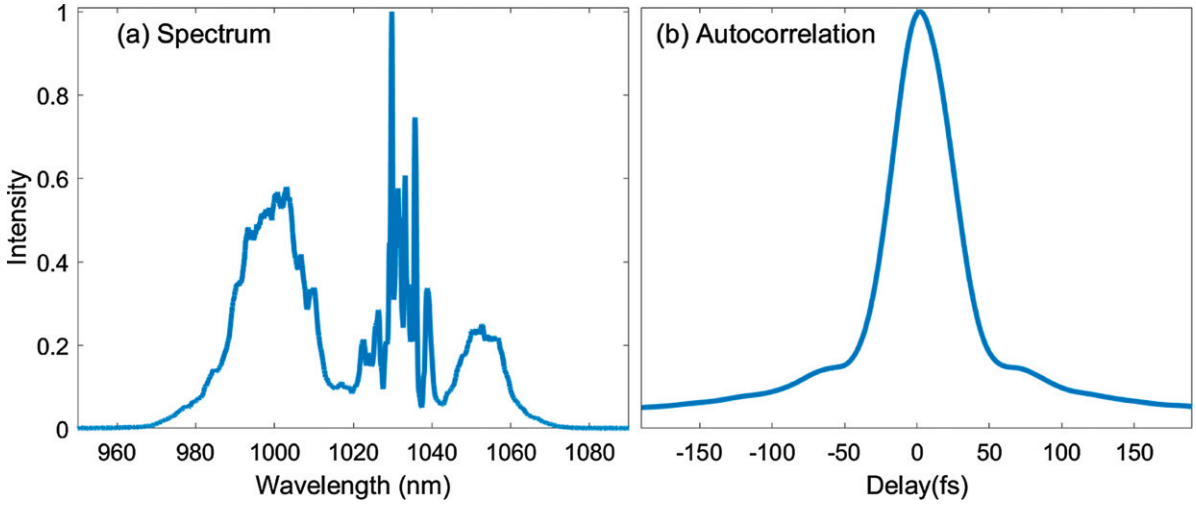

Figure 2. Driving laser parameters used for recording the RABBITT trace. (a) The spectrum. (b) Intensity autocorrelation of ∼40 fs pulse.

average power. There are two methods to filter a high-average-power driving beam. One uses materials, such as SiO_2 plates, that reflect XUV radiation in grazing incidence and transmit the driving laser pulses [78, 86, 87]. The other method makes use of annular beams to generate high-order harmonics [88]. Due to the intrinsic highly nonlinear nature of the HHG process, the wavefronts of the XUV radiation and of the driving laser are different in the generation area [89–93], so that they have notable differences in divergence and spatial shape. Therefore, they can be separated spatially after propagation in the generating medium [70, 94, 95]. The phases of the high-order harmonics from different trajectories of the same photon energy are also different [54, 90, 96], so an annular spatial block can be used to filter the generating laser beam as well as high harmonic contributions from the long trajectories [97–99]. By blocking the central part of a beam with a gaussian-like shape, an annular beam can be formed and is used to generate high-order harmonics [48, 88, 100]. In order to characterize the temporal shape of the high-order harmonics and for pump-probe experiments, the central part can be utilized. There are three configurations of using annular beam for attosecond pulse production. In annular-type-1, the laser is separated temporally to a central beam and an annular beam by a delay plate with an annular shape. The two beams are combined temporally by the other plate, and are focused into the gas jet [1, 101]. In annular-type-2, the laser is seperated spatially by a holey mirror to a transmitted central beam and a reflected annular beam. The two beams are combined before HHG and are focused by a lens to gas jet [102]. In these two types, the attosecond pulse overlaps with the probe beam at its birth. In our case in the HR-GHHG beamline of ELI-ALPS, annular-type-3, the laser is also separated by a holey mirror to two, however, in order to use high average power and provide more flexibility to control the probe beam, the IR probe pulses and the attosecond pulses are recombined after HHG [9, 103].

Due to the aforementioned difficulties, to the best of our knowledge, until now very few groups reported on the temporal characterization of the attosecond pulses produced at high repetition rates. Hammerland *et al* [104] transported their beamline to ELI-ALPS and measured the duration of the attosecond pulse train in the presence of interfering dressing fields using the HR-1 laser (fiber-CPA) of ELI-ALPS. Osolodkov *et al* [51] used OPCPA to generate few-pulse attosecond pulse trains and used SiO_2 plates [78] and metal filter to attenuate the driving laser.

In this work, by combining cutting edge high repetition rate laser technology and unique configuration of the HR-GHHG beamline using annular beam at ELI-ALPS, we generated and delivered attosecond pulses at 100 kHz with the flux of 2.8×10^{10} XUV photons per second on target. The duration is measured to be 395 as using the technique of RABBITT. To date, these are the highest flux attosecond pulses delivered to target produced via HHG in argon driven by a high-repetition-rate 1030 nm fiber-CPA laser. The realization of the attosecond pulse train at 100 kHz at our beamline is an important milestone for future experiments that ELI-ALPS can offer and host. These experiments will benefit from the high repetition rate of attosecond pulses.

2. HR-GHHG beamline in ELI-ALPS

The HR-1 laser at ELI-ALPS [105] was used as the driving source in this work. It combines the technologies of fiber-CPA and hollow-core fiber (HCF) nonlinear pulse compression [106]. The central wavelength is 1030 nm. The repetition rate of the laser pulses from a fiber oscillator is decreased to 100 kHz by two acousto-optic modulators. The laser is amplified in large-pitch fibers (LPFs, 65 μm core diameter, 1 m length) to 20 W. It is subsequently divided into eight beams for amplification in eight LPFs, which are pumped by high-power continuous-wave diodes. The eight channels are coherently combined into one beam of 200 fs with 300 W power, which is further compressed temporally by two stages of HCFs and chirped mirrors to the duration between 20 fs to 100 fs with 80 W power. The laser system at different stages of development is described in detail in references [83, 107]. In this paper,

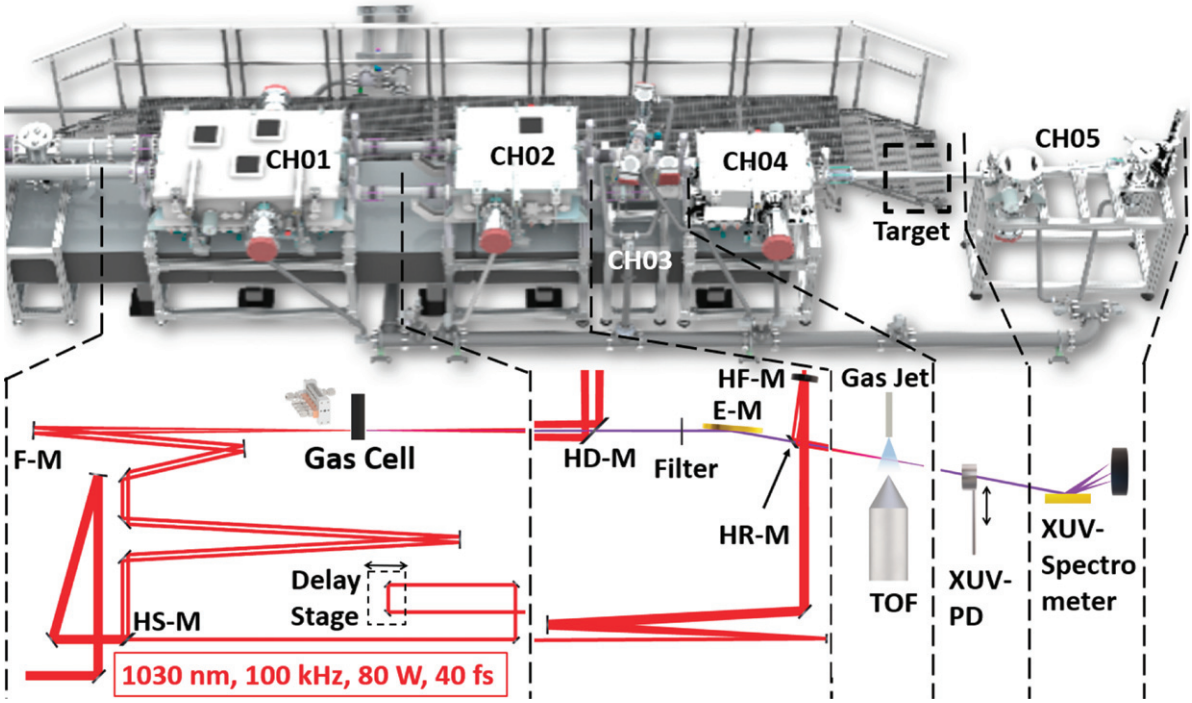

Figure 3. The HR-GHHG beamline at ELI-ALPS. Top: the 3D model. The complete beamline is under vacuum. Bottom: the simulated beam paths using ray-tracing in Zemax. Red line is the driving laser. The purple line is the generated XUV radiation. Details can be found in the main text.

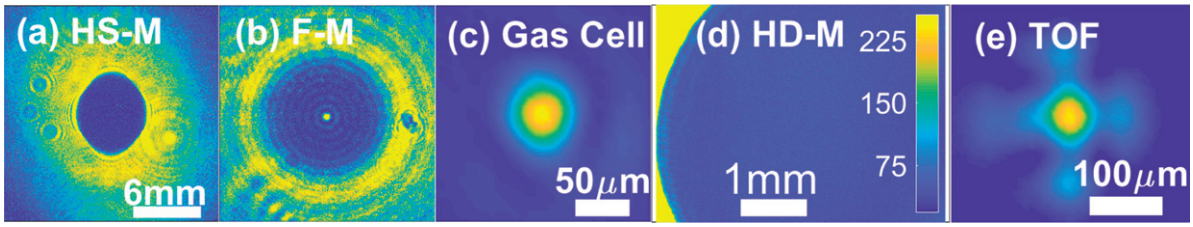

Figure 4. The beam profiles of the IR laser (a) on the holey-splitting mirror (HS-M), (b) in front of the focusing mirror (F-M), (c) in the focus at the gas cell, (d) at the position of the holey-dump mirror (HD-M), and (e) at entrance of the TOF. (a) and (b) were obtained by imaging the spatial profiles of the laser beam at the corresponding planes onto the detector of the camera. (c)–(e) were recorded by directly putting the camera at the corresponding planes.

XUV pulses were generated and measured using 40 fs driving pulses, as shown in figure 2(b), along with the IR spectrum (figure 2(a)).

The 3D representation of the HR-GHHG beamline and a functional schematic of each section of the experimenal setup is presented in figure 3. In the following, the driving laser is called IR (infrared), and the high-order harmonics are called XUV (extreme ultraviolet). In the first chamber (CH01) the IR is split into a reflected annular beam (used for XUV generation) (figure 4(a)) and a transmitted central beam by a holey-splitting mirror (HS-M) with a hole diameter of 6 mm. The reflected part propagates to the focusing mirror (F-M) of 900 mm focal length, where the beam profile can be seen in figure 4(b), and it is focused into a gas cell to generate high-order harmonics. The beam profile of the IR at focus is shown in figure 4(c). The home-made water-cooled gas cell has a 10 mm length and a 1.4 mm entrance hole diameter [108].

After the gas cell the generation beam propagates through a 6 mm-diameter holey dump mirror (HD-M). In order to get an annular beam at HD-M without obvious diffraction rings in the center, HS-M and HD-M were set to be the object and the image of the F-M, respectively. Part of the annular beam is recorded using a CCD camera (figure 4(d)). The hole is represented by the central blue part. The annular beam, seen in the left corner, is shown in yellow (the CCD is saturated), and it is reflected by the HD-M into a beam dump outside the vacuum chamber. The generated XUV (purple line in figure 3) is transmitted through the central hole of the HD-M and is focused by an ellipsoidal mirror (E-M) to the entrance of a time-of-flight (TOF) spectrometer (Stefan Kaesdorf GmbH ETF11). The central IR beam propagating through the hole of the HS-M and that is not used for XUV generation is expanded and collimated by two spherical mirrors after a delay-line, and is focused by a holey-focusing mirror (HF-M) to the entrance of

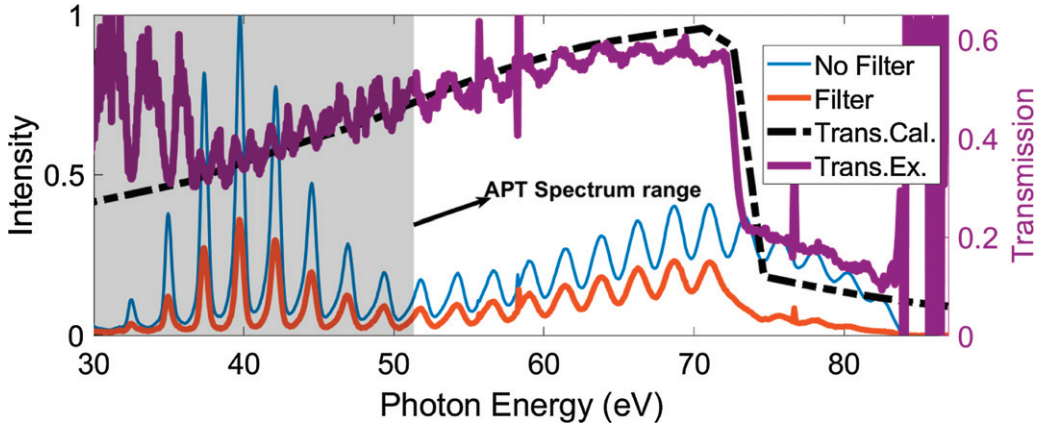

Figure 5. High-order harmonics generated by 20 fs laser for calibration of the energy axis of the XUV spectrometer. Blue (red) line is the measured spectrum of high-harmonics without (with) filter. The black dotted line is the caculated transmission of 86 nm Al and 14 nm Al_2O_3. The purple line is the measured transmission of the filter. The gray shaded area marks the photon energy range of the APT, which is generated by 40 fs laser.

the TOF spectrometer (figure 4(e)). The holey-recombination mirror (HR-M) is a flat mirror with a hole in the center, allowing the XUV beam passing through. The two pulsed beams are overlapped at the entrance of the TOF both spatially and temporally in vacuum chamber CH03. The TOF spectrometer collects the electrons resulting from the ionization by the XUV in the presence of the IR. As shown in figure 3, leaving the volume at the entrance of the TOF spectrometer in CH03, the XUV beam is focused by a toroidal mirror in the 4th chamber (CH04) onto the target area, where the end stations for different applications can be placed. Such applications involve photoelectron emission spectroscopy (PES), reaction microscope (REMI), transient absorption spectroscopy or velocity map imaging (VMI) [9]. In the CH04, the XUV beam hits the retractable XUV photodiode (XUV-PD) (NIST 40790C) for pulse energy measurement. The photodiode is absolutely calibrated in the 5–120 nm wavelength region. The device is a fused silica disk with a thin film (about 150 nm) of aluminum oxide deposited. It is totally blind to the IR radiation, therefore it provides a true measure of XUV flux independently on the residual IR that is transmitted toward the spectrometer. When the XUV-PD is moved out of the beam path, the XUV propagates to the XUV spectrometer in 5th chamber (CH05), in which the XUV is dispersed and focused by a variable line spacing grating (HITACHI 001-0437) to a microchannel plate(MCP, type Photek VID140). A CMOS camera (IDS 3060) is used to record the image on the phosphor screen behind the MCP. The total response of the utilized MCP and grating combination is studied by Poletto *et al* [109].

3. Experimental results

In this section we describe the optimization process of the high-order harmonics and the measurement of the temporal shape and the flux of the APT.

3.1. HHG using an annular beam at 100 kHz

Before optimizing the HHG for high-flux APT production, we calibrate the XUV spectrometer. In order to reach the absorption edge of Al at 72 eV, the duration of the generating laser is decreased to 20 fs. As shown in figure 5, the 72 eV absorption edge of the Al filter and the 53 eV cooper minimum [110, 111] in argon can be seen clearly and can be used for photon energy calibration. The nominal thickness of the Al filter is 100 nm. Assuming that the filter consists of 86 nm Al and 14 nm Al_2O_3, one can calculate the transmission of the filter (black dotted line) which matches the measured transmission (purple line) in the photon energy range betwee 35 eV and 70 eV. The argon gas is used in TOF to characterize the APT. The ionization cross section of argon decreases very fast above 50 eV and the detection efficiency is low. Due to this reason, we increased the driving pulse duration to 40 fs, and optimized the high-order harmonic generation efficiency in the range below 50 eV, marked in figure 5 as the gray and transparent area.

We moved the gas cell to the position, defined as 0 mm, to reach the highest cutoff. As shown in figure 6(a), at the fixed position of 0 mm, the intensity of the high-order harmonics increases with the backing pressure. The highest intensity was obtained at the backing pressure of 390 mbar, which was the highest pressure due to the limit of pumping capacity. Fixing the pressure and moving the gas cell, we can decrease the photon energy below 50 eV at the position of ∼4.1 mm marked by a white dotted line in figure 6(b), where we optimized the high harmonic generation for APT as described in the next section.

3.2. Attosecond pulse train at 100 kHz repetition rate

The XUV APT and the IR beams were focused together into the argon gas jet of the TOF spectrometer (CH03 in figure 3) ensuring spatial and temporal overlap. The interaction of Ar atoms with both XUV and IR light fields generates electron wave packets. The peaks in the generated photoelectron spectrum correspond to the existing ionization channels. Without the IR the measured electron spectrum showed a shape similar to that of the XUV photon spectrum where only the odd harmonic orders can be observed. The peaks correspond to single-photon ionization induced by the XUV APT. With the IR field included, additional photoionization channels open up (XUV

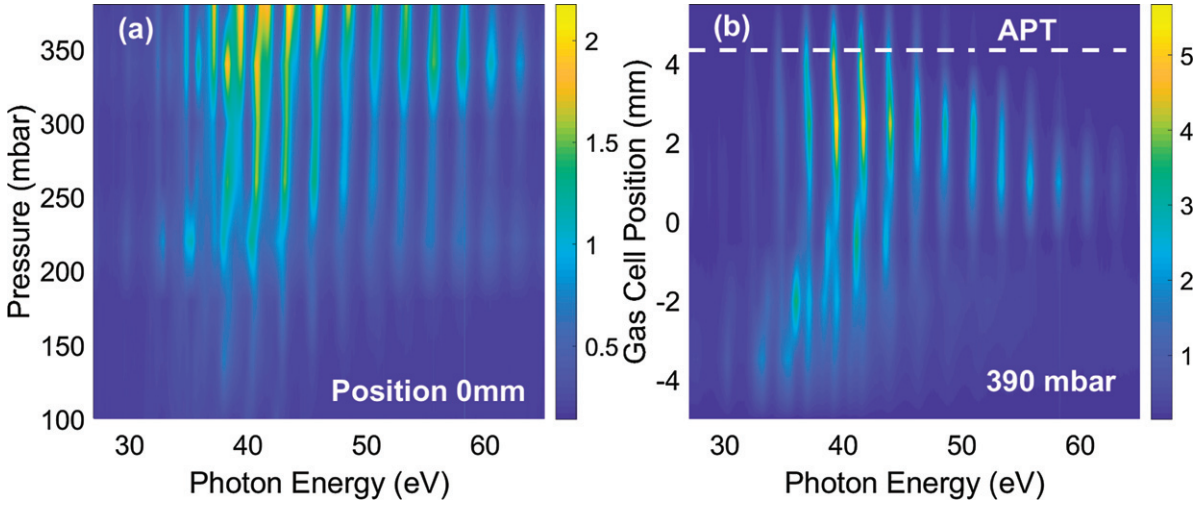

Figure 6. High-order harmonics generated by the 100 kHz laser. (a) Pressure scan: the spectra were recorded as a function of backing pressure, with a relative position of the gas cell at 0 mm, giving the highest cut-off in the experiments with the 40 fs laser pulse. The static pressures in the gas cell corresponding to the backing pressure highlighted in the figure were estimated to be between 33 mbar and 130 mbar. (b) Gas cell position scan. The backing pressure was set to 390 mbar.

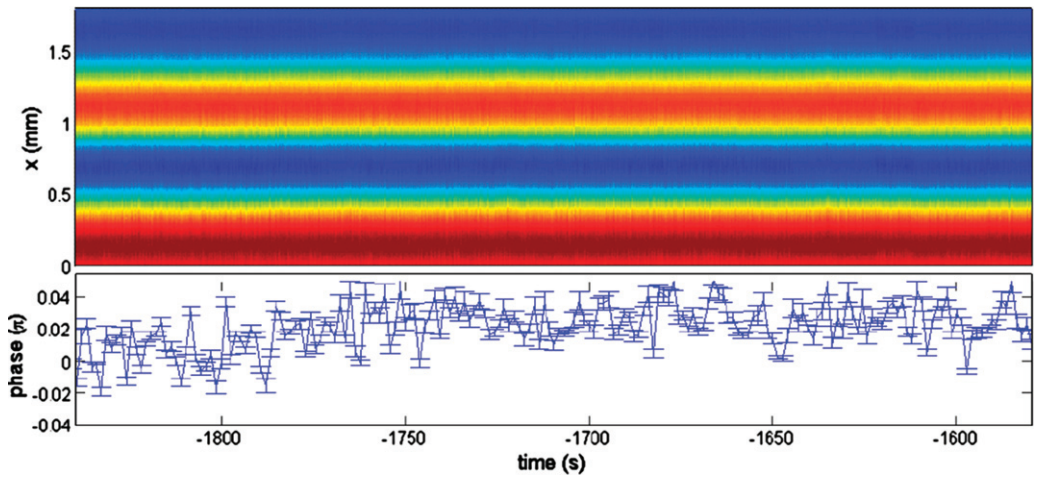

Figure 7. Fluctuation of the path difference of XUV arm and IR arm. Top: the interference fringes of the He–Ne laser. Bottom: the phase extracted from the top picture ($0.01\pi \sim 10.1$ as). The STD is 14.2 ± 0.4 as.

$\pm$ IR), giving rise to the delay-dependent additional peaks of even orders in the photoelectron spectrum, called sidebands. Each sideband of even order q has four quantum paths contributions representing the four different two-photon ionization channels: (1) absorbing one $(q-1)$th harmonic and then absorbing an IR photon; (2) absorbing an IR photon and then absorbing one $(q-1)$th harmonic; (3) emitting an IR photon and then absorbing one $(q+1)$th harmonic; (4) absorbing one $(q+1)$th harmonic and then emitting an IR photon. The interference among those quantum paths results in delay-dependent oscillation of the sidebands, from which the intensity profile of the APT can be reconstructed.

The stability of the delay (path difference between XUV and IR) is essential for the accurate measurement of the RABBITT trace. A delay fluctuation below 50 as is needed to measure a pulse duration of hundreds of attoseconds. In collinear [2] configuration the two beams propagate through the same path, so the relative fluctuation of the two arms is minimized. In this work, a non-collinear configuration was used (figure 3). In order to analyze the delay-stability of the XUV-IR interferometer, a He–Ne laser was employed, which was aligned to propagate along the same paths as the IR and XUV beams. The He–Ne laser beam was split in CH01 and recombined in CH04 (see figure 3). The interference fringes of the two beams were recorded using a CCD camera. As shown in figure 7, the standard deviation (STD) of the path difference of the two arms can be as low as 14.2 ± 0.4 as within 200 s of measurement time. The typical value of the STD was sub-40 as.

Figure 8(a) shows the measured RABBITT trace, from which the relative phases of the high-order harmonics can be obtained [1, 66, 112]. Figure 8(b) shows the electron spectrum with and without IR beam, and the phase of the high-order

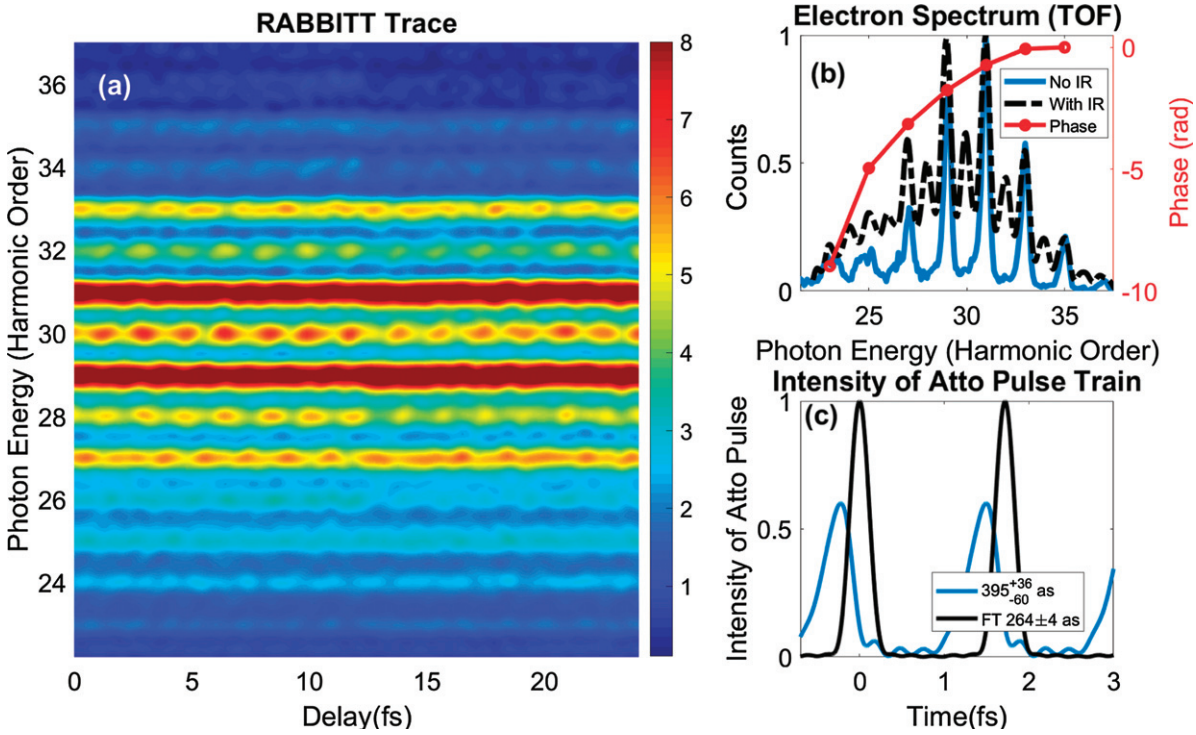

Figure 8. Reconstruction of the attosecond pulse train. (a) The RABBITT trace. The integration time of each delay point was 5 s and the delay step was 133 as. (b) The electron TOF spectrum ionized by the APT without and with the IR probe. Red dots show the phase of the harmonics extracted from (a). (c) The reconstructed APT from the measurement (blue curve) and the Fourier transform limited APT (black curve).

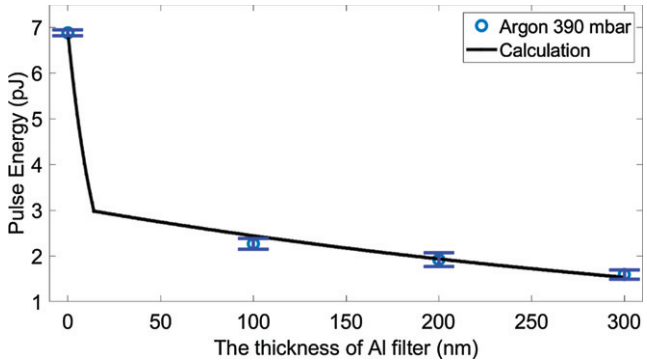

Figure 9. Flux measurement of the APT. The photon energy range was from 25 eV to 50 eV. The blue circles show the pulse energy of the APT with different thickness of the filters. The black line is calculated according to the transmission of the filter.

harmonics. Figure 8(c) shows the reconstructed average pulse in APT with a duration of 395^{+36}_{-60} as. The transform-limited duration is 264 ± 4 as, showing the chirp of the pulse train.

The XUV-PD in CH04, shown in figure 3, was inserted to measure the pulse energy of the APT. When the average power of the laser was 80 W, the XUV APT pulse energies were measured to be 6.8 pJ without filter and 2 pJ with 100 nm Al filter (see figure 9). In addition to the previous two situations, we analyzed the filter transmission as a function of filter thickness. In this analysis, the D is the nominal thickness of the Al filter and d is the thickness of the Al_2O_3 formed by oxidation on the two surfaces of Al foil. The oxidation of Al is assumed to have stopped when the thickness of Al_2O_3 reached 7 nm on one surface. Previous works from other groups show similar level of oxidation, i.e. that the thickness of Al_2O_3 on one surface of a bulk material is in the order of several nanometers [47, 113, 114]. The black curve is the calculated pulse energy transmitted through the Al filter with a nominal thickness of D and it matches the experiment data (blue circle). As shown in figure 1, for the HHG driving by 1030 nm and 100 kHz fiber-CPA laser in argon, we measured the highest HHG pulse energy delivered to target until now.

4. Discussion

4.1. The attenuation of the high-order harmonics from generation to target

A 'clean' high-order harmonic beam not overlapped with the driving laser beam is essential for many applications. Several methods have been used to remove the driving laser from the co-propagating beams, as mentioned in the introduction. Here we used an annular IR beam to generate high-order harmonics, so driving beam can be spatially separated from the generated XUV beam by a holey dump mirror after the generation, as shown in figure 3. Only a thin filter is needed to filter out the residual laser. Based on theoretical calculations, the attenuation of a 100 nm Al filter around 40 eV is ∼21%. However, because of the oxidation the measured attenuation is ∼70%. Until now, this has been the lowest attenuation from generation to the target for high-order harmonics driven by a laser

of high repetition rate and high average power (∼100 W) [45, 51]. When an un-oxidized Al filter is used, an attenuation as low as ∼21% is expected from generation to target.

4.2. Efficiency of HHG

The energy conversion efficiency is estimated as 1.8×10^{-8}, by taking into account the transmission of the Al filter and the reflections from the XUV mirrors. The efficiency of HHG in argon using 800 nm laser at similar repetition rates can achieve 1×10^{-6} [47]. The harmonic-generation efficiency is known to have a wavelength dependence giving a scaling of $\sim\lambda^{-6}$ [115, 116]. Based on the above two values, the efficiency of HHG using 1030 nm laser could reach $\sim 3 \times 10^{-7}$. Our energy conversion efficiency is approximately one order of magnitude lower than what can be expected with these parameters. Two main factors limited the efficiency in our system. The first one is the temporal shape of the pulse. The autocorrelation trace (see figure 2) shows a low pedestal in the range of 100 fs, so the energy was not fully concentrated in the main pulse. The pulses with better temporal contrast can improve the generation efficiency. We are developing the laser system in this aspect. One of the key points in laser development is the characterization of laser pulses with complex temporal structures, for example using the method introduced in one of our recent publications [117].

The second factor is the pressure of the generation medium. The coherence length L_{coh} of qth order harmonic is the propagation distance after which the phase of qth harmonic changes by π. The absorption length L_{abs} is the propagation distance where the intensity of the harmonic drop by e^{-1} due to the absorption. In the case of absorption-limited high-order harmonics generation, the flux is optimized when $L_{\mathrm{m}} > 3L_{\mathrm{abs}}$ and $L_{\mathrm{coh}} > 5L_{\mathrm{abs}}$, where L_{m} is the length of the generation medium [118]. In argon at the pressure of 130 mbar, L_{abs} of the harmonics around 40 eV photon energy is ∼3.2 mm. The coherence length L_{coh} is ∼0.5 mm, assuming a focused IR beam the waist of 40 μm (corresponding to the experimental situation, see figure 4(c)). The gas pressure can be increased to decrease the absorption length, and a focusing mirror with longer focusing length can be applied to increase the coherence length, and hence absorption-limited HHG can be achieved. This is in-line with our observation that a higher medium pressure can lead to higher XUV flux (depicted in figure 6(a)), but our current system is limited to the pressure range reported here.

In summary a higher flux can be expected by using shorter generating laser pulses, by increasing the pressure of the generation medium, and by using longer focal length optics for the generation. Nonetheless, a global optimization using all the control parameters is essential for extracting the best output from the beamline [119].

5. Conclusion

We reported on the first measurements from the HR-GHHG 100 kHz beamline at ELI-ALPS. We demonstrated the generation of attosecond pulse trains at 100 kHz repetition rate, with an average duration of 395 as, pulse energy of 2 pJ, and flux of 2.8×10^{10} photons per second on target. The high harmonic flux can be optimized in several ways, by tailoring phase-matching conditions by adjusting the focusing geometry and adapting the gas density profile in the generation medium. All these are topics for future work. The current results are achieved by taking advantage of the unique properties of the 100 kHz fiber-CPA system combined with an annular driving beam generation geometry. The 100 kHz attosecond pulse source opens applicability for experiments in needs of more events per second to get high signal-to-noise ratio and higher flux on target, such as microscopy, time-resolved photoelectron emission spectroscopy, and coincidence measurements. This result is a milestone toward attosecond science with a high repetition rate.

Acknowledgments

The ELI-ALPS project (GINOP-2.3.6-15-2015-00001) is supported by the European Union and co-financed by the European Regional Development Fund. CV, MD, ML, MN and SS acknowledge support by the Italian Ministry of Research and Education with the projects ELI ESFRI Roadmap. DC acknowledges support by 'HELLAS-CH' (MIS Grant No. 5002735) co-financed by Greece and the European Regional Development Fund. AZ acknowledges the support of UKRI EPSRC through projects EP/J002348/1 and 2319767.

ORCID iDs

Peng Ye https://orcid.org/0000-0002-5697-2509
Tamás Csizmadia https://orcid.org/0000-0001-5969-9846
Lénárd Gulyás Oldal https://orcid.org/0000-0003-2852-9945
Miklós Füle https://orcid.org/0000-0001-6996-2329
Tímea Grósz https://orcid.org/0000-0001-8345-1007
Balázs Major https://orcid.org/0000-0001-5981-340X
Fabio Frassetto https://orcid.org/0000-0001-5528-1995
Giacinto Davide Lucarelli https://orcid.org/0000-0002-8188-0753
Matteo Lucchini https://orcid.org/0000-0001-6476-100X
Bruno Moio https://orcid.org/0000-0001-9649-7362
Salvatore Stagira https://orcid.org/0000-0002-8457-3185
Caterina Vozzi https://orcid.org/0000-0002-0212-0191
Mauro Nisoli https://orcid.org/0000-0003-2309-732X
Subhendu Kahaly https://orcid.org/0000-0001-7600-3310
Amelle Zaïr https://orcid.org/0000-0003-1687-5453
Katalin Varjú https://orcid.org/0000-0001-6577-7417

References

[1] Paul P M, Toma E S, Breger P, Mullot G, Auge F, Balcou P, Muller H G and Agostini P 2001 *Science* **292** 1689–92
[2] Hentschel M, Kienberger R, Spielmann C, Reider G, Milosevic N, Brabec T, Corkum P, Heinzmann U, Drescher M and Krausz F 2001 *Nature* **414** 509–13
[3] Gallmann L, Cirelli C and Keller U 2012 *Annu. Rev. Phys. Chem.* **63** 447–69
[4] Frank F *et al* 2012 *Rev. Sci. Instrum.* **83** 52

[5] Rudawski P *et al* 2013 *Rev. Sci. Instrum.* **84** 073103
[6] Dubrouil A, Hort O, Catoire F, Descamps D, Petit S, Mével E, Strelkov V and Constant E 2014 *Nat. Commun.* **5** 4637
[7] Gaumnitz T, Jain A, Pertot Y, Huppert M, Jordan I, Ardana-Lamas F and Wörner H J 2017 *Opt. Express* **25** 27506–18
[8] Li J *et al* 2017 *Nat. Commun.* **8** 186
[9] Kühn S *et al* 2017 *J. Phys. B: At. Mol. Opt. Phys.* **50** 132002
[10] Serkez S, Geloni G, Tomin S, Feng G, Gryzlova E, Grum-Grzhimailo A and Meyer M 2018 *J. Opt.* **20** 024005
[11] Hartmann N *et al* 2018 *Nat. Photon.* **12** 215
[12] Drescher M, Hentschel M, Kienberger R, Uiberacker M, Yakovlev V, Scrinzi A, Westerwalbesloh T, Kleineberg U, Heinzmann U and Krausz F 2002 *Nature* **419** 803
[13] Itatani J, Levesque J, Zeidler D, Niikura H, Pépin H, Kieffer J C, Corkum P B and Villeneuve D M 2004 *Nature* **432** 867–71
[14] Uiberacker M *et al* 2007 *Nature* **446** 627
[15] Schultze M *et al* 2010 *Science* **328** 1658–62
[16] Pazourek R, Nagele S and Burgdörfer J 2015 *Rev. Mod. Phys.* **87** 765
[17] Calegari F *et al* 2014 *Science* **346** 336–9
[18] Nisoli M, Decleva P, Calegari F, Palacios A and Martín F 2017 *Chem. Rev.* **117** 10760–825
[19] Ossiander M *et al* 2017 *Nat. Phys.* **13** 280
[20] Chen C *et al* 2017 *Proc. Natl Acad. Sci. USA* **114** E5300–7
[21] Stockman M I, Kling M F, Kleineberg U and Krausz F 2007 *Nat. Photon.* **1** 539
[22] Hommelhoff P and Kling M F 2015 *Attosecond Nanophysics* (New York: Wiley) p 13
[23] Förg B *et al* 2016 *Nat. Commun.* **7** 11717
[24] Seiffert L *et al* 2017 *Nat. Phys.* **13** 766–70
[25] Kim K T, Zhang C, Shiner A D, Schmidt B E, Légaré F, Villeneuve D and Corkum P 2013 *Nat. Photon.* **7** 958
[26] Garg M, Zhan M, Luu T T, Lakhotia H, Klostermann T, Guggenmos A and Goulielmakis E 2016 *Nature* **538** 359
[27] Eckle P, Pfeiffer A, Cirelli C, Staudte A, Dörner R, Muller H, Büttiker M and Keller U 2008 *Science* **322** 1525–9
[28] Zaïr A *et al* 2013 *Chem. Phys.* **414** 184–91
[29] Wörner H J, Bertrand J B, Kartashov D V, Corkum P B and Villeneuve D M 2010 *Nature* **466** 604
[30] Attar A R, Bhattacherjee A, Pemmaraju C, Schnorr K, Closser K D, Prendergast D and Leone S R 2017 *Science* **356** 54–9
[31] Frasinski L, Codling K and Hatherly P 1989 *Science* **246** 1029–31
[32] Tsatrafyllis N, Kominis I, Gonoskov I and Tzallas P 2017 *Nat. Commun.* **8** 15170
[33] Tsatrafyllis N *et al* 2019 *Phys. Rev. Lett.* **122** 193602
[34] Frasinski L, Giles A, Hatherly P, Posthumus J, Thompson M and Codling K 1996 *J. Electron Spectrosc. Relat. Phenom.* **79** 367–71
[35] Frasinski L *et al* 2013 *Phys. Rev. Lett.* **111** 073002
[36] Palacios A, González-Castrillo A and Martín F 2014 *J. Phys. B: At. Mol. Opt. Phys.* **47** 124013
[37] Cattaneo L, Vos J, Bello R Y, Palacios A, Heuser S, Pedrelli L, Lucchini M, Cirelli C, Martín F and Keller U 2018 *Nat. Phys.* **14** 733–8
[38] Dörner R, Mergel V, Jagutzki O, Spielberger L, Ullrich J, Moshammer R and Schmidt-Böcking H 2000 *Phys. Rep.* **330** 95–192
[39] Buss J H *et al* 2019 *Rev. Sci. Instrum.* **90** 023105
[40] Hädrich S, Krebs M, Rothhardt J, Carstens H, Demmler S, Limpert J and Tünnermann A 2011 *Opt. Express* **19** 19374–83
[41] Pupeza I *et al* 2013 *Nat. Photon.* **7** 608
[42] Lorek E, Larsen E W, Heyl C M, Carlström S, Paleček D, Zigmantas D and Mauritsson J 2014 *Rev. Sci. Instrum.* **85** 123106
[43] Ozawa A, Zhao Z, Kuwata-Gonokami M and Kobayashi Y 2015 *Opt. Express* **23** 15107–18
[44] Emaury F, Diebold A, Saraceno C J and Keller U 2015 *Optica* **2** 980–4
[45] Rothhardt J *et al* 2016 *Opt. Express* **24** 18133–47
[46] Labaye F *et al* 2017 *Opt. Lett.* **42** 5170–3
[47] Harth A *et al* 2017 *J. Opt.* **20** 014007
[48] Klas R, Kirsche A and Tschernajew M 2018 Rothhardt J and Limpert J *Opt. Express* **26** 19318–27
[49] Porat G, Heyl C M, Schoun S B, Benko C, Dörre N, Corwin K L and Ye J 2018 *Nat. Photon.* **12** 387–91
[50] Saule T *et al* 2019 *Nat. Commun.* **10** 1–10
[51] Osolodkov M, Furch F J, Schell F, Susnjar P, Cavalcante F, Menoni C S, Schulz C P, Witting T and Vrakking M J 2019 arXiv:1908.07744
[52] Krausz F and Ivanov M 2009 *Rev. Mod. Phys.* **81** 163
[53] Chatziathanasiou S *et al* 2017 *Photonics* **4** 26
[54] Nayak A *et al* 2019 *Phys. Rep.* **833** 1–52
[55] Corkum P B 1993 *Phys. Rev. Lett.* **71** 1994–7
[56] Lewenstein M, Balcou P, Ivanov M Y, L'Huillier A and Corkum P B 1994 *Phys. Rev.* A **49** 2117–32
[57] Popmintchev T *et al* 2012 *Science* **336** 1287–91
[58] Teichmann S M, Silva F, Cousin S, Hemmer M and Biegert J 2016 *Nat. Commun.* **7** 11493
[59] Johnson A S *et al* 2018 *Sci. Adv.* **4** eaar3761
[60] Sansone G *et al* 2006 *Science* **314** 443–6
[61] Mikkelsen A *et al* 2009 *Rev. Sci. Instrum.* **80** 123703
[62] Calegari F, Liu C, Lucchini M, Sansone G and Nisoli M 2013 Gating techniques for shaping of attosecond pulses *Progress in Ultrafast Intense Laser Science* (Berlin: Springer) pp 55–69
[63] Chini M, Zhao K and Chang Z 2014 *Nat. Photon.* **8** 178
[64] Haessler S *et al* 2009 *Phys. Rev.* A **80** 011404
[65] Huppert M, Jordan I, Baykusheva D, Von Conta A and Wörner H J 2016 *Phys. Rev. Lett.* **117** 093001
[66] Isinger M, Busto D, Mikaelsson S, Zhong S, Guo C, Salières P, Arnold C, L'Huillier A and Gisselbrecht M 2019 *Phil. Trans. R. Soc.* A **377** 20170475
[67] Kasmi L, Lucchini M, Castiglioni L, Kliuiev P, Osterwalder J, Hengsberger M, Gallmann L, Krüger P and Keller U 2017 *Optica* **4** 1492–7
[68] Locher R, Castiglioni L, Lucchini M, Greif M, Gallmann L, Osterwalder J, Hengsberger M and Keller U 2015 *Optica* **2** 405–10
[69] Lucchini M *et al* 2015 *Phys. Rev. Lett.* **115** 137401
[70] Hammond T, Brown G G, Kim K T, Villeneuve D and Corkum P 2016 *Nat. Photon.* **10** 171
[71] Mills A K, Zhdanovich S, Sheyerman A, Levy G, Damascelli A and Jones D J 2015 *Proc. SPIE* **9512** 95121I
[72] Lindner F, Stremme W, Schätzel M G, Grasbon F, Paulus G G, Walther H, Hartmann R and Strüder L 2003 *Phys. Rev.* A **68** 013814
[73] Wang H, Xu Y, Ulonska S, Robinson J S, Ranitovic P and Kaindl R A 2015 *Nat. Commun.* **6** 7459
[74] Krebs M, Hädrich S, Demmler S, Rothhardt J, Zaïr A, Chipperfield L, Limpert J and Tünnermann A 2013 *Nat. Photon.* **7** 555
[75] Guo C *et al* 2017 Compact 200 kHz HHG source driven by a few-cycle OPCPA *Conf. on Lasers and Electro-Optics Europe and European Quantum Electronics Conference* (*CLEO/Europe-EQEC*) (Munich, Germany)
[76] Timmers H, Sabbar M, Hellwagner J, Kobayashi Y, Neumark D M and Leone S R 2016 *Optica* **3** 707–10
[77] Calegari F, Vozzi C, Negro M, Sansone G, Frassetto F, Poletto L, Villoresi P, Nisoli M, De Silvestri S and Stagira S 2009 *Opt. Lett.* **34** 3125–7
[78] Hädrich S, Klenke A, Rothhardt J, Krebs M, Hoffmann A, Pronin O, Pervak V, Limpert J and Tünnermann A 2014 *Nat. Photon.* **8** 779

[79] Chiang C T, Huth M, Trützschler A, Kiel M, Schumann F O, Kirschner J and Widdra W 2015 *New J. Phys.* **17** 013035
[80] Cabasse A, Hazera C, Quintard L, Cormier E, Petit S and Constant E 2016 *J. Phys. B: At. Mol. Opt. Phys.* **49** 085601
[81] Hädrich S *et al* 2016 *Opt. Lett.* **41** 4332–5
[82] Gonzalez A I *et al* 2018 *J. Opt. Soc. Am.* B **35** A6–14
[83] Nagy T *et al* 2019 *Optica* **6** 1423–4
[84] Mero M, Heiner Z, Petrov V, Rottke H, Branchi F, Thomas G M and Vrakking M J 2018 *Opt. Lett.* **43** 5246–9
[85] Witting T, Furch F J and Vrakking M J 2018 *J. Opt.* **20** 044003
[86] Takahashi E J, Hasegawa H, Nabekawa Y and Midorikawa K 2004 *Opt. Lett.* **29** 507–9
[87] Nagata Y, Nabekawa Y and Midorikawa K 2006 *Opt. Lett.* **31** 1316–8
[88] Peatross J, Chaloupka J and Meyerhofer D 1994 *Opt. Lett.* **19** 942–4
[89] Corkum P B 1993 *Phys. Rev. Lett.* **71** 1994
[90] Lewenstein M, Balcou P, Ivanov M Y, L'huillier A and Corkum P B 1994 *Phys. Rev.* A **49** 2117
[91] Salieres P, L'Huillier A and Lewenstein M 1995 *Phys. Rev. Lett.* **74** 3776–9
[92] Ye P, Teng H, He X K, Zhong S Y, Wang L F, Zhan M J, Zhang W, Yun C X and Wei Z Y 2014 *Phys. Rev.* A **90** 063808
[93] Wikmark H *et al* 2019 *Proc. Natl Acad. Sci. USA* **116** 4779–87
[94] Hickstein D D *et al* 2015 *Nat. Photon.* **9** 743
[95] Zhong S, He X, Jiang Y, Teng H, He P, Liu Y, Zhao K and Wei Z 2016 *Phys. Rev.* A **93** 033854
[96] Salières P *et al* 2001 *Science* **292** 902–5
[97] Gaarde M B, Salin F, Constant E, Balcou P, Schafer K, Kulander K and L'Huillier A 1999 *Phys. Rev.* A **59** 1367
[98] Zair A *et al* 2008 *Phys. Rev. Lett.* **100** 143902
[99] Ye P, He X, Teng H, Zhan M, Zhong S, Zhang W, Wang L and Wei Z 2014 *Phys. Rev. Lett.* **113** 073601
[100] Gaumnitz T, Jain A and Wörner H J 2018 *Opt. Lett.* **43** 4506–9
[101] Zaïr A, Mével E, Cormier E and Constant E 2018 *J. Opt. Soc. Am.* B **35** A110–5
[102] Mairesse Y *et al* 2003 *Science* **302** 1540–3
[103] Reduzzi M *et al* 2015 *Phys. Rev.* A **92** 033408
[104] Hammerland D *et al* 2019 *J. Phys. B: At. Mol. Opt. Phys.* **52** 23LT01
[105] https://eli-alps.hu/
[106] Nisoli M, De Silvestri S and Svelto O 1996 *Appl. Phys. Lett.* **68** 2793–5
[107] Hädrich S *et al* 2016 *Opt. Lett.* **41** 4332–5
[108] Filus Z 2020 in preparation
[109] Poletto L, Tondello G and Villoresi P 2001 *Rev. Sci. Instrum.* **72** 2868–74
[110] Cooper J W 1962 *Phys. Rev.* **128** 681
[111] Higuet J *et al* 2011 *Phys. Rev.* A **83** 053401
[112] Muller H G 2002 *Appl. Phys.* B **74** s17–21
[113] Erny C, Mansten E, Gisselbrecht M, Schwenke J, Rakowski R, He X, Gaarde M, Werin S and L'Huillier A 2011 *New J. Phys.* **13** 073035
[114] Revie R W 2008 *Corrosion and Corrosion Control: An Introduction to Corrosion Science and Engineering* (New York: Wiley) p 383
[115] Sansone G, Poletto L and Nisoli M 2011 *Nat. Photon.* **5** 655
[116] Shiner A, Trallero-Herrero C, Kajumba N, Bandulet H C, Comtois D, Légaré F, Giguère M, Kieffer J, Corkum P and Villeneuve D 2009 *Phys. Rev. Lett.* **103** 073902
[117] Gulyás Oldal L, Csizmadia T, Ye P, Harshitha N, Füle M and Zaïr A 2019 *Appl. Phys. Lett.* **115** 051106
[118] Constant E, Garzella D, Breger P, Mével E, Dorrer C, Le Blanc C, Salin F and Agostini P 1999 *Phys. Rev. Lett.* **82** 1668
[119] Kovács K *et al* 2019 *J. Phys. B: At. Mol. Opt. Phys.* **52** 055402